Structure of the *Escherichia coli* Fumarate Reductase Respiratory Complex

Tina M. Iverson,[1] César Luna-Chavez,[2] Gary Cecchini,[2]* Douglas C. Rees[3]*

The integral membrane protein fumarate reductase catalyzes the final step of anaerobic respiration when fumarate is the terminal electron acceptor. The homologous enzyme succinate dehydrogenase also plays a prominent role in cellular energetics as a member of the Krebs cycle and as complex II of the aerobic respiratory chain. Fumarate reductase consists of four subunits that contain a covalently linked flavin adenine dinucleotide, three different iron-sulfur clusters, and at least two quinones. The crystal structure of intact fumarate reductase has been solved at 3.3 angstrom resolution and demonstrates that the cofactors are arranged in a nearly linear manner from the membrane-bound quinone to the active site flavin. Although fumarate reductase is not associated with any proton-pumping function, the two quinones are positioned on opposite sides of the membrane in an arrangement similar to that of the Q-cycle organization observed for cytochrome bc_1.

Because oxygen has a high affinity for electrons, aerobic respiration represents a very favorable form of energy metabolism. However, in the absence of oxygen, many microorganisms can obtain energy through anaerobic respiratory processes that result in the reduction of alternate terminal acceptors (*1*). One of the most widespread acceptors is fumarate (*2*), which is reduced to succinate by fumarate reductase, an integral membrane protein containing flavin adenine dinucleotide (FAD) and iron-sulfur clusters (*3*). The electron donor for this reaction is reduced menaquinone, which commonly serves as a membrane-soluble, mobile electron carrier between respiratory complexes. The most extensively characterized fumarate reductase, from *Escherichia coli*, has a total molecular mass of 121 kD in four subunits. It consists of two water-soluble subunits, the flavoprotein (66 kD) and iron-sulfur protein (27 kD) subunits, and two membrane anchor subunits (15 and 13 kD), which are the products of the *frdABCD* genes, respectively (*4*). The flavoprotein (Fp) subunit contains the catalytic site for fumarate reduction and succinate oxidation at a covalently linked FAD (*5*), while the iron-sulfur protein subunit (Ip) contains three different types of iron-sulfur clusters, [2Fe:2S], [4Fe:4S], and [3Fe:4S], which have been spectroscopically characterized (*6*). At least two sites associated with the membrane anchor subunits have been proposed to bind the quinones that are involved in electron transfer reactions of the enzyme (*7*).

Fumarate reductase catalyzes the reverse reaction of succinate dehydrogenase, which participates in both the aerobic respiratory chain as complex II and in the Krebs cycle (*3*). These two proteins exhibit substantial similarities in amino acid sequence, cofactor composition, and mechanism. Indeed, under certain conditions, one enzyme can functionally replace the other and support bacterial growth (*8*). Because of the central role of fumarate reductase and succinate dehydrogenase in respiration, mutations in these complexes can have substantial metabolic consequences. In bacteria, mutations in fumarate reductase can significantly retard growth under appropriate conditions (*9*). In higher organisms, mutations of succinate dehydrogenase have been linked to oxidative stress and aging in nematodes (*10*) and to Leigh's syndrome in humans (*11*). Historically, succinate dehydrogenase was one of the most widely studied enzymes during the development of enzymology. Early studies resulted in the discoveries of nonheme iron and covalently bound flavin in proteins (*12*). To provide a framework for addressing the functional properties of fumarate reductase and succinate dehydrogenase, we have solved the structure of the *E. coli* fumarate reductase at 3.3 Å resolution. Here we describe the fold of the polypeptides and location of the cofactors, and the functional implications of this structural arrangement.

[1]Graduate Option in Biochemistry, 147-75CH, California Institute of Technology, Pasadena, CA 91125, USA. [2]Molecular Biology Division, Department of Veterans Affairs Medical Center, San Francisco, CA 94121, and Department of Biochemistry and Biophysics, University of California, San Francisco, CA 94143, USA. [3]Howard Hughes Medical Institute, Division of Chemistry and Chemical Engineering, 147-75CH, California Institute of Technology, Pasadena, CA 91125, USA.

*To whom correspondence should be addressed. E-mail: ceccini@itsa.ucsf.edu; dcrees@caltech.edu

Structure Determination and Overall Fold

Fumarate reductase from *E. coli* was purified and crystallized in the presence of the nonionic detergent Thesit (*13*). The structure was solved by multiple wavelength anomalous diffraction (MAD), with data collected at three wavelengths near the Fe K edge (*14*) (Table 1). The iron-sulfur clusters and transmembrane helices were striking in the initial maps calculated at 4 Å resolution, and the structure was solved by iterative combination of density modification, noncrystallographic symmetry averaging, model building, and refinement (*15*). The final model has been refined to values of R_{cryst} of 22.2% and R_{free} of 29.2% at 3.3 Å resolution with reasonable stereochemistry (*15*, *16*).

The four subunits in fumarate reductase are arranged in a complex resembling the letter "q," with the top of the "q" generated by the Fp and Ip subunits (diameter ~70 Å), while the tail of the "q" (length 110 Å) contains the membrane anchor subunits (Fig. 1, A and B). The orientation of fumarate reductase in the cell membrane is such that the Fp and Ip subunits are located in the cytoplasm (equivalent to the mitochrondrial matrix for succinate dehydrogenase). In these crystals, two fumarate reductase complexes, which are related by a twofold axis approximately parallel to the membrane normal, are present per asymmetric unit. These two complexes associate through their transmembrane regions. Contacts with neighboring molecules related by crystallographic symmetry also occur in the membrane-spanning region, creating a continuous membrane-spanning region throughout the crystal (Fig. 1C). Despite the suggestiveness of this arrangement, there is no evidence that a dimer is physiologically relevant, unlike the situation with cytochrome bc_1 (*17*). Additionally, the contact region between fumarate reductase molecules in the crystals is relatively small (~325 Å^2) (*18*) and is unlikely to support formation of a stable dimer (Fig. 1B).

The Fp (FrdA) subunit is organized around an FAD/NAD(P) (nicotinamide adenine dinucleotide phosphate) binding domain formed by residues A1 to A50, A130 to A231, and A354 to A414 (Fig. 2A). This domain structure includes a Rossmann-type fold that provides the binding site for FAD. The FAD is further associated with the flavoprotein through a covalent bond between the flavin C8A methyl group and the Nε atom of the side chain of His A44. The remaining residues of this subunit, A51 to A129, A232 to A353, and A415 to A575, are inserted into

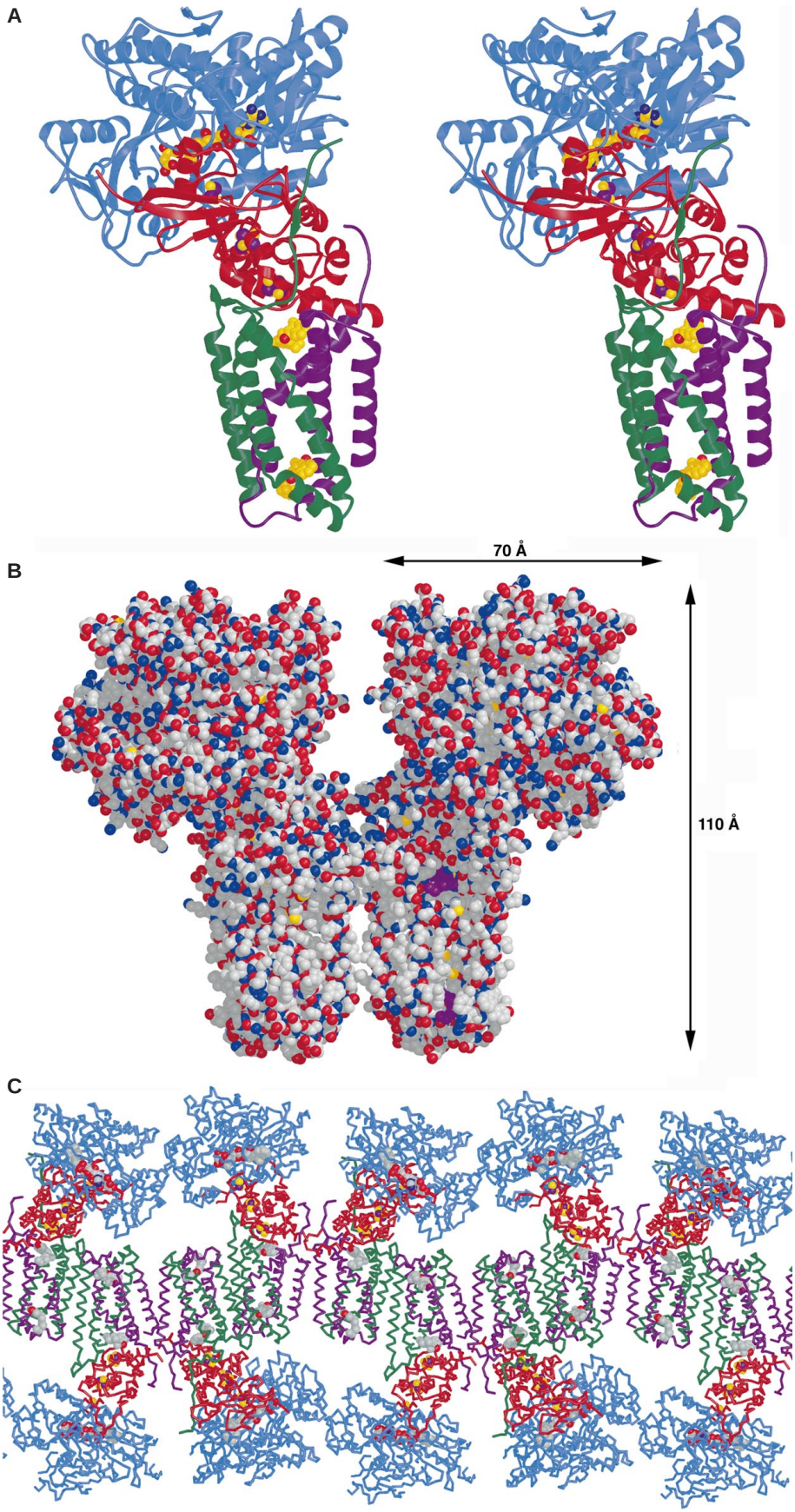

Fig. 1. Structure of fumarate reductase. (**A**) Stereoview of a fumarate reductase monomer. The flavoprotein is in blue, the iron protein is in red, and the membrane anchors are in green (FrdC) and purple (FrdD). The [Fe:S] clusters are shown as purple (Fe atoms) and yellow (S atoms), while the menaquinones and FAD are shown in yellow. (**B**) Space-filling model of fumarate reductase showing the crystal contacts between the two complexes in the membrane-spanning portion. In the fumarate reductase complex, oxygen atoms are shown in red, nitrogen atoms are shown in blue, sulfur atoms are shown in yellow. Menaquinone molecules are shown in magenta (see right-hand monomer). The location of the membrane-spanning region can be inferred from the coloring of the atoms in this representation. The more hydrophilic (soluble) region contains many polar oxygen and nitrogen atoms (red and blue) while the hydrophobic (membrane-spanning) region contain mostly apolar carbon atoms (gray). (**C**) Crystal packing of fumarate reductase is through the transmembrane regions of the protein (green and purple) and forms a continuous membrane-spanning portion in the crystal (*36*). In this representation, the FAD and menaquinone are shown in gray (*37*).

the core FAD binding domain and adopt compact folds that do not exhibit significant structural similarities to known folds in the Protein Data Bank, as assessed by the DALI server (*19*).

Fumarate reductase contains three iron-sulfur clusters that are coordinated by cysteine residues in the Ip (FrdB) subunit as follows: [2Fe:2S] (Cys residues B57, B62, B65, and B77); [4Fe:4S] (Cys B148, B151, B154, and B214); and [3Fe:4S] (Cys B158, B204, and B210). Consistent with the conclusions of sequence and electron paramagnetic resonance (EPR) analyses (*3*, *6*), the Ip subunit is organized into two domains (Fig. 2B), one characteristic of [2Fe:2S]-containing ferredoxins (residues B1 to B91) and the other characteristic of bacterial ferredoxins that contain [3Fe:4S] or [4Fe:4S] type clusters (residues B145 to B221). The [2Fe:2S] domain superimposes closely with plant-type ferredoxins, while more substantial changes have occurred in the bacterial ferredoxin domain. Although bacterial ferredoxins containing both a [3Fe:4S] and a [4Fe:4S] cluster are relatively common, the cysteine ligands for the [3Fe:4S] cluster always appear first in the protein sequence. As anticipated from sequence analyses, the cluster arrangement in fumarate reductase is reversed relative to these ferredoxins. In addition, the four-stranded antiparallel β sheet found on one side of the clusters in ferredoxins has been replaced by a helical hairpin in fumarate reductase.

The two membrane anchor subunits, FrdC and FrdD, exhibit similar folds, each with three transmembrane helices connected by extra-membrane loops (Fig. 2C). These helices, designated I to VI (*3*), consist of residues C22 to C49, which is actually composed of two kinked, helical segments, C66 to C90, C105 to C128, D9 to D35, D61 to D89, and D97 to D115, and are in reasonable agreement with transmembrane segments predicted by hydropathy analysis and mutagenesis (*20*). Helices I, II, IV, and V are tilted ~30° to 40° from the membrane normal, as defined by the dimer twofold axis, and are arranged in a right-handed, helical bundle, with helix crossing angles of ~120°. In contrast, helices III and VI are more parallel to the membrane normal with a tilt of ~10° to 25°. The NH_2- and COOH-termini are on opposite sides of the membrane-spanning region, which correspond to the cytoplasm and periplasm, respectively. The overall arrangement is such that the two subunits could be covalently connected upon deletion of helix III, consistent with the observation that homologous enzymes have been identified that contain only a single transmembrane domain with five membrane-spanning helices (*20*).

Two menaquinone molecules, which are located on opposite sides of the membrane-spanning region, are present in this fumarate reductase structure. The menaquinone (Q_P) positioned proximal to the [3Fe:4S] cluster of the Ip subunit binds in a relatively polar pocket formed by helices I, II, IV, and V, while the second menaquinone (Q_D) distal to this cluster, is positioned ~27 Å from the first and binds in a relatively hydrophobic pocket near the other ends of helices I, II, IV, and V. Site-directed mutagenesis and labeling with azido-quinones have implicated residues in both these regions as involved in quinone binding in both fumarate reductase and succinate dehydrogenase (*9*, *21*). Although evidence suggests that complex II contains a stabilized semiquinone pair in close proximity to the [3Fe-4S] cluster with the quinone rings perpendicular to the membrane plane (*7*, *22*), only single quinone molecules were identified at the spatially distinct Q_P and Q_D sites in the fumarate reductase structure. In the absence of a conformational rearrangement of the protein in the Q_P region, it does not appear that this site can accommodate more than one quinone molecule.

Redox Centers and Electron Transfer Pathway

The six redox cofactors of fumarate reductase are organized into a chain with the sequence FAD-[2Fe:2S]-[4Fe:4S]-[3Fe:4S]-Q_P-Q_D (Fig. 3). With the exception of the ~27 Å spacing between the two menaquinones, the redox cofactors are all separated by ~11 to 14 Å center-to-center distances, which are common cofactor separation distances observed in multicentered electron transfer proteins. In its physiologically relevant reaction, electrons enter fumarate reductase in the form of reduced menaquinone, although the enzyme will physiologically reduce ubiquinone at rates similar to native succinate dehydrogenase (*8*). Examination of a space-filling model of fumarate reductase indicates that both quinone binding sites are exposed and should be accessible to the exterior of the complex (Fig. 1B). Electron transfer to the iron-sulfur cluster almost certainly would occur from the Q_P site, which is adjacent to the [3Fe:4S] cluster. Although Q_P primarily interacts with residues from both membrane anchor subunits, it has limited contact with Ip through Lys B238. The polar environment of the Q_P (Fig. 4A) site resembles the Q_B site of bacterial photosynthetic reaction centers (*23*), which can accommodate all three quinone oxidation states (reduced, oxidized, and semiquinone). The Q_D site has an apolar character (Fig. 4B) that resembles the Q_A site of photosynthetic reaction centers, which can accommodate only the oxidized and semiquinone states. Indeed, residues in the Q_P and Q_D binding pockets had been identified with Q_B and Q_A, respectively, based on the consequences of residue substitution (*7*). However, the assignments of quinone oxidation states to specific binding sites during enzyme turnover cannot be unambiguously established at present.

During fumarate reduction, electrons from reduced quinone are transferred to the iron-sulfur clusters. Both the oxygen sensitivity upon removal of the membrane anchor subunits and perturbation of the EPR spectrum of the [3Fe:4S] cluster by quinone site inhibitors and mutants suggest that the [3Fe:4S] cluster interacts with the quinone binding subunits to initially accept electrons from the menaquinone (*9*, *24*). Spectroscopic studies have indicated that the [2Fe:2S] cluster is in close proximity to the FAD (*25*), and this cluster is the likely donor of electrons to the flavin. The crystallographic structure demonstrates that His A44, covalently linked to the flavin, intervenes between the flavin and [2Fe:2S] cluster. Although there was speculation that the [4Fe:4S] cluster was "off-pathway," in part due to the low reduction potential of this center, the structure confirms the proposal from EPR studies that the clusters are arranged in the sequence [3Fe:4S]-[4Fe:4S]-[2Fe:2S] (*6*). The consequences of this arrangement for kinetics of electron transfer through complex II have recently been discussed (*26*).

Many of the residues observed to participate in the binding of FAD to fumarate reductase had been previously identified from sequence analysis, and from molecular biological and biochemical studies. The binding site for fumarate can be inferred from the location of oxaloacetate observed in the structure. Oxaloacetate is a physiological inhibitor of fumarate reductase (inhibition constant $K_i < 1$ μM), and purified preparations of enzyme contain oxaloacetate that remains

Table 1. Summary of data collection and refinement statistics. Numbers in parentheses indicate values for the highest resolution bin. The figure of merit was 0.48 for all data to 4.0 Å. $R_{sym} = \Sigma|I_i - \langle I\rangle|/\Sigma[\langle I\rangle|$. Res, resolution (in angstroms); URef, number of unique reflections; and Red, redundancy. ⟨PP⟩ denotes overall phasing power to 4 Å resolution.

Energy (keV)	f'	f''	Res	URef	Red	Completeness (%)	R_{sym}	I/σ	⟨PP⟩
7.500 (high remote)	−2.2	3.6	3.3	49,332	4.4	87.2 (90.0)	0.093 (0.277)	15.1 (6.3)	2.6
7.127 (peak)	−6.6	4.5	3.5	39,139	5.3	94.1 (91.0)	0.096 (0.236)	14.5 (7.9)	2.8
7.120 (inflection)	−4.2	2.7	4.0	31,125	4.1	97.2 (97.1)	0.118 (0.269)	15.8 (10.2)	1.6

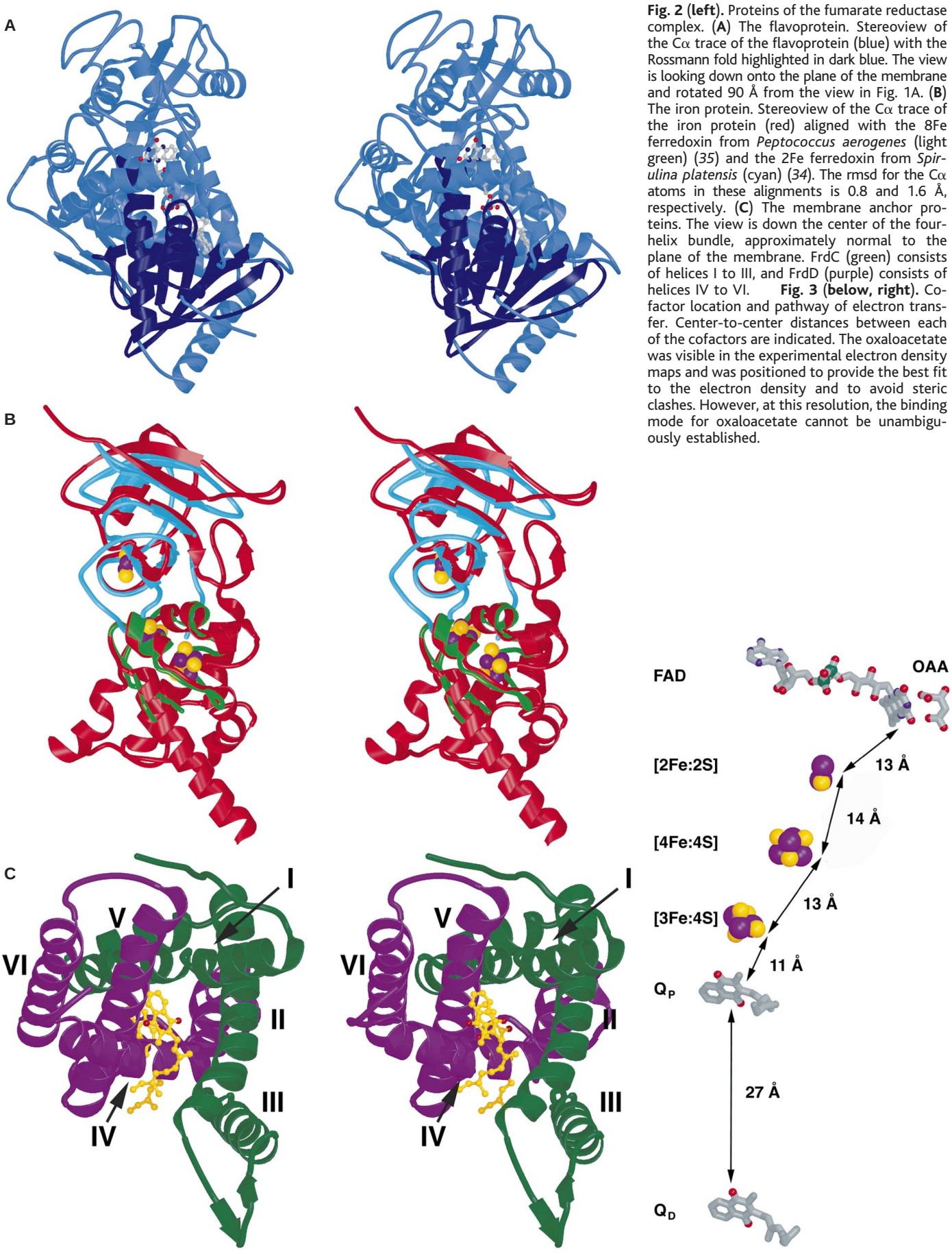

Fig. 2 (left). Proteins of the fumarate reductase complex. (**A**) The flavoprotein. Stereoview of the Cα trace of the flavoprotein (blue) with the Rossmann fold highlighted in dark blue. The view is looking down onto the plane of the membrane and rotated 90 Å from the view in Fig. 1A. (**B**) The iron protein. Stereoview of the Cα trace of the iron protein (red) aligned with the 8Fe ferredoxin from *Peptococcus aerogenes* (light green) (*35*) and the 2Fe ferredoxin from *Spirulina platensis* (cyan) (*34*). The rmsd for the Cα atoms in these alignments is 0.8 and 1.6 Å, respectively. (**C**) The membrane anchor proteins. The view is down the center of the four-helix bundle, approximately normal to the plane of the membrane. FrdC (green) consists of helices I to III, and FrdD (purple) consists of helices IV to VI. **Fig. 3 (below, right).** Cofactor location and pathway of electron transfer. Center-to-center distances between each of the cofactors are indicated. The oxaloacetate was visible in the experimental electron density maps and was positioned to provide the best fit to the electron density and to avoid steric clashes. However, at this resolution, the binding mode for oxaloacetate cannot be unambiguously established.

bound until an excess of substrate is added (*27*). Oxaloacetate interacts with a pocket of arginines and histidines near the side of the flavin opposite to the [2Fe:2S] cluster (Fig. 4C). This group is positioned near conserved residues His A232, Glu A245, and His A355, which may serve as proton donors, and the N5 of the flavin, which likely functions as a hydride donor to fumarate. Although the flavin is buried, access to the active site could take place at the interface between two domains of the Fp.

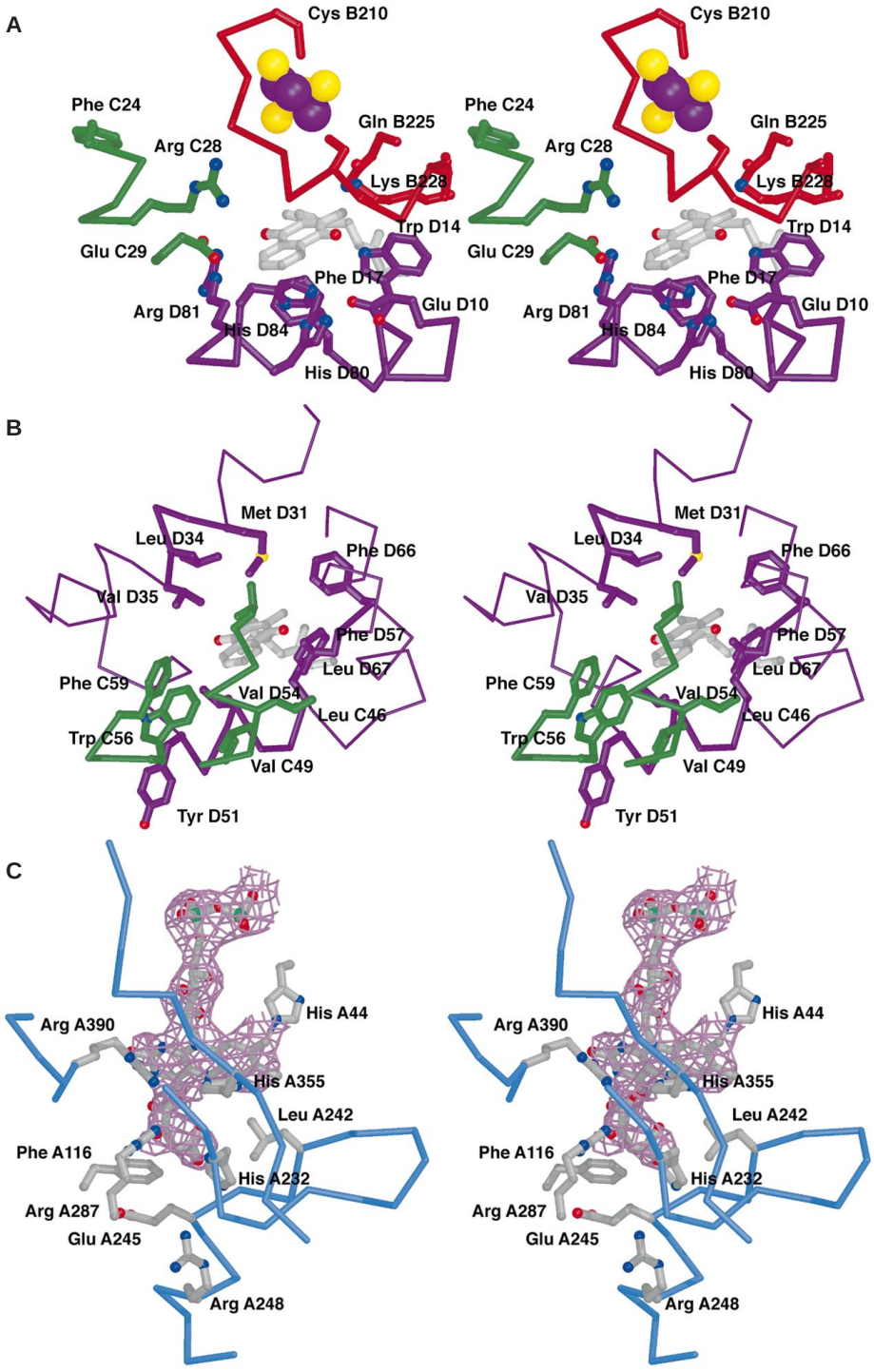

Fig. 4. Quinone binding pockets and active site residues. (**A**) Stereoview of the Q_P binding site shows Q_P is bound in a polar pocket likely positioned just above the membrane bilayer. (**B**) Stereoview of the Q_D site shows Q_D is in a relatively apolar pocket within the membrane bilayer. (**C**) Binding site for the physiological inhibitor oxaloacetate adjacent to the FAD. Oxaloacetate lies beneath the isoalloxazine ring of the flavin. The flavin ring and inhibitor are shown superimposed onto a $2|F_o| - |F_c|$ map contoured at 1σ. The adenine has been omitted for clarity. Side chains that appear to interact directly with the inhibitor are labeled.

Implications for Energy Transduction Processes in Respiration

Quinones play a central role in respiration because they serve as membrane-soluble electron carriers that can couple proton and electron transfer reactions. In the placement of quinones on opposite sides of the membrane-spanning region, fumarate reductase resembles the arrangement observed in cytochrome bc_1 (*17*) more than the photosynthetic reaction center (*23*), where the quinones are on the same side of the membrane. This distinction can be functionally significant, because the quinone arrangement in cytochrome bc_1 (*17*) allows proton translocation to be coupled to electron transfer through operation of the Q-cycle, as first recognized by Mitchell (*28*). When quinones are on opposite sides of the membrane, the Q-cycle couples oxidation at one quinone site to reduction at the second site, with the net result that protons are transported across the membrane. In contrast, if the quinones are on the same side of the membrane as in the reaction center (*23*), there may be proton release associated with hydroquinone oxidation, or proton uptake associated with quinone oxidation, but there cannot be quinone-mediated proton translocation across the membrane. In cytochrome bc_1, two heme groups are positioned between the quinone binding sites to mediate electron transfer between these centers. While the *E. coli* fumarate reductase lacks heme, other fumarate reductases and succinate dehydrogenases contain one or two b-type hemes. These hemes are likely coordinated by histidine residues positioned between the quinone sites in the membrane-spanning region. Although fumarate reductase and succinate dehydrogenase are not known to couple proton translocation to electron transfer, the similar arrangement of redox groups across the membrane like that found in the cytochrome bc_1 complex raises the possibility that at some point these enzymes may have participated in proton translocation.

Fumarate reductase and succinate dehydrogenase occupy central positions in cellular energy metabolism; fumarate reductase serves as the terminal acceptor for a major anaerobic respiratory pathway, while succinate dehydrogenase participates in both the Krebs cycle and as complex II of the aerobic respiratory chain. Although fumarate reductase and succinate dehydrogenase catalyze the same reaction (but in different physiological directions) and are predicted to have similar structures, organisms with both types of respiratory chains use distinct proteins for each purpose for reasons not understood. In terms of the overall process of respiration, exciting progress has been made recently in structurally characterizing membrane-associated members of respiratory pathways (*29*). Fumarate reductase

(complex II) now joins structures available for cytochrome bc_1 [complex III (*17*)], cytochrome c oxidase [complex IV (*30*)], and the F_1 component of the ATP synthase [complex V (*31*)]. This gives a more complete view of the respiratory chain at the atomic level and increases our understanding of one of the most fundamental processes of biological systems.

References and Notes

1. For a review, see G. Gottschalk, *Bacterial Metabolism* (Springer-Verlag, New York, ed. 2, 1986).
2. For a review, see A. Kröger, V. Geisler, E. Lemma, F. Theis, R. Lenger, *Arch. Microbiol.* **158**, 311 (1992).
3. For reviews, see B. A. C. Ackrell, M. K. Johnson, R. P. Gunsalus, G. Cecchini, in *Chemistry and Biochemistry of Flavoenzymes*, F. Müller, Ed. (CRC Press, Boca Raton, FL, 1992), vol. 3, pp. 229–297; C. Hägerhäll, *Biochim. Biophys. Acta* **1320,** 107 (1997); J. J. Van Hellemond and A. G. M. Tielens, *Biochem. J.* **304**, 321 (1994).
4. T. Grundström and B. Jaurin, *Proc. Natl. Acad. Sci. U.S.A.* **79**, 1111 (1982); S. T. Cole, *Eur. J. Biochem.* **122**, 479 (1982); _____, T. Grundström, B. Jaurin, J. J. Robinson, J. H. Weiner, *ibid.* **126**, 211 (1982).
5. W. H. Walker and T. P. Singer, *J. Biol. Chem.* **245**, 4224 (1970); J. H. Weiner and P. Dickie, *Can. J. Biochem.* **254**, 8590 (1979).
6. J. E. Morningstar, M. K. Johnson, G. Cecchini, B. A. C. Ackrell, E. B. Kearney, *J. Biol. Chem.* **260**, 13631 (1985); R. Cammack, D. S. Patil, J. H. Weiner, *Biochim. Biophys. Acta* **870**, 545 (1986); A. T. Kowal *et al.*, *Biochemistry* **34**, 12284 (1995).
7. F. J. Ruzicka, H. Beinert, K. L. Schepler, W. R. Dunham, R. H. Sands, *Proc. Natl. Acad. Sci. U.S.A.* **72**, 2886 (1975); J. C. Salerno and T. Ohnishi, *Biochem. J.* **192**, 769 (1980); D. J. Westenberg, R. P. Gunsalus, B. A. C. Ackrell, H. Sices, G. Cecchini, *J. Biol. Chem.* **268**, 815 (1993).
8. E. Maklashina, D. K. Berthold, G. Cecchini, *J. Bacteriol.* **180**, 5989 (1998); J. R. Guest, *J. Gen. Microbiol.* **122**, 171 (1981).
9. J. H. Weiner *et al.*, *Proc. Natl. Acad. Sci. U.S.A.* **83**, 2056 (1986); G. Cecchini *et al.*, *ibid.*, p. 8898; D. J. Westenberg, R. P. Gunsalus, B. A. C. Ackrell, G. Cecchini, *J. Biol. Chem.* **265**, 19560 (1990); I. Schröder, R. P. Gunsalus, B. A. C. Ackrell, B. Cochran, G. Cecchini, *ibid.* **266**, 13572 (1991).
10. N. Ishii *et al.*, *Nature* **394**, 694 (1998).
11. T. Bourgeron *et al.*, *Nature Genet.* **11**, 144 (1995).
12. T. P. Singer, *Biological Oxidations*, T. P. Singer, Ed. (Interscience, New York, 1968), pp. 339–377.
13. Fumarate reductase from *E. coli* was produced and purified as described (C. Luna-Chavez and G. Cecchini, in preparation). In brief, protein was extracted into 0.05% (w/v) Thesit (polyoxyethylene 9-dodecyl ether) and concentrated to 30 mg/ml in a buffer of 20 mM tris (pH 7.4) and 0.7% Thesit. Crystals were obtained by vapor diffusion with hanging drops equilibrated against a reservoir solution [8% PEG 10,000, 0.1 M sodium citrate (pH 5.8), 0.085 M magnesium acetate, 0.1 mM EDTA, 0.001% (w/v) dithiothreitol]. Menaquinone and oxaloacetate were not added to either the protein preparation or the crystallization conditions. Crystals grew in the space group $P2_12_12_1$ with unit cell constants $a = 96.6$ Å, $b = 138.1$ Å, and $c = 275.3$ Å and two complexes per asymmetric unit. The oxidation state of the enzyme cannot be clearly established in this structure.
14. Data were collected by the inverse beam method at −180°C at beam line 5.0.2 at the Advanced Light Source with an ADSC Quantum4 charge-coupled device. Wavelengths for optimal data collection were determined with a single-crystal EXAFS (extended x-ray absorption fine structure) scan. Data were processed with DENZO and scaled with SCALEPACK [Z. Otwinoski and W. Minor, *Methods Enzymol.* **276**, 307 (1997)] and the CCP4 suite of programs (*32*).
15. Sites for the iron-sulfur clusters were determined from anomalous Patterson maps calculated at 6 Å resolution with the program FFT (*32*). Positions and occupancies of the sites, as well as values for f′ and f″ for two wavelengths, were refined with the program SHARP [E. De La Fortelle and G. Bricogne, *Methods Enzymol.* **276A**, 472 (1997)] yielding initial phases. Phases were improved with solvent flattening and multiple domain noncrystallographic averaging in DM [(*32*); K. Cowtan, *Joint CCP4 EACBM Newslett. Crystallogr.* **31**, 34 (1994)] initially with the transformation matrix determined based on the positions of the iron-sulfur clusters with the program FINDNCS [G. Lu, *J. Appl. Crystallogr.* **32**, 365 (1999)]. Masks used in averaging were calculated with MAMA [G. J. Kleywegt and T. A. Jones, *Acta Crystallogr.* **D55**, 941 (1999)]. The model was built as a polyalanine chain at 4 Å resolution with the program O version 6.22 [T. A. Jones and M. Kjeldgaard, *Methods Enzymol.* **277**, 173 (1997)]. Subsequent rounds of modeling used the structures of NADH peroxidase [Protein Data Bank (PDB) accession number 1joa.pdb; the root mean square deviation (rmsd) is 1.4 Å for the 125 Cα atoms in this alignment] (*33*), the 2Fe ferredoxin from *Spirulina platensis* (accession number 4fxc.pdb) (*34*), and the 8Fe ferredoxin from *Peptococcus aerogenes* (accession number 1fdx.pdb) (*35*) as guides for structurally similar regions. This modeling used phase-combined maps produced by SIGMAA (*32*) and REFMAC [(*32*); G. N. Murshudov, A. A. Vagin, E. J. Dodson, *Acta Crystallogr.* **D53**, 240 (1997)]. Side chains were added to the model when the effective resolution reached 3.5 Å resolution and the R_{free} dropped below 40%. Side chain assignment in the iron protein was greatly aided by sequence analysis identifying the iron-sulfur cluster ligands (*3*). Side chains were initially assigned to the flavoprotein based on sequence similarity with NADH peroxidase in the flavin-binding region. Refinement was carried out with alternating cycles of REFMAC [(*32*); G. N. Murshudov, A. A. Vagin, E. J. Dodson, *Acta Crystallogr.* **D53**, 240 (1997)] and X-PLOR [N. S. Pannu and R. J. Read, *ibid.* **A52**, 659 (1996)] with tight noncrystallographic symmetry (NCS) restraints on the soluble region until the R_{free} dropped below 35%, when the NCS restraints were only loosely used. The rmsd of the soluble and membrane domains of the two NCS related complexes in the asymmetric unit is 0.85 and 0.79 Å, respectively, as determined with the program LSQKAB (*32*). To take advantage of the quality and completeness of the peak data set and the higher resolution of the high remote data set, we chose the same test set for R_{free} for these data sets and alternated refinement between them. The values for R_{cryst} and R_{free} after refinement are 22.2 and 29.2%, respectively, where $R_{cryst} = \Sigma||F_o| - |F_c||/\Sigma|F_o|$ and R_{free} is R_{cryst} for 2% of the reflections omitted from the refinement totaling 1005 Bijvoet pairs. The rmsd of bond lengths and angles is 0.02 Å and 1.9°, respectively, with less than 1% of the residues having disallowed values for the Φ and Ψ angles according to a Ramachandran diagram. The final model for each complex contains 8467 atoms in residues 1 to 575 (of 601 total residues) of FrdA, 1 to 243 (of 243 total residues) of FrdB, 1 to 130 (of 130 total residues) of FrdC, and 1 to 118 (of 118 residues) of FrdD, as well as a [2Fe:2S] cluster, a [3Fe:4S] cluster, a [4Fe:4S] cluster, a FAD, an oxaloacetate molecule, two menaquinone molecules, and one molecule of ordered detergent. The initiator methionine has been excluded from residue numbering because it is believed to be cleaved from the mature protein (*3*), consistent with the lack of electron density seen before residue 1 of each protein in the complex.
16. The coordinates have been deposited in the Protein Data Bank (accession number 1fum).
17. D. Xia *et al.*, *Science* **277**, 60 (1997); Z. Zhang *et al.*, *Nature* **392**, 677 (1998); S. Iwata *et al.*, *Science* **281**, 64 (1998).
18. Surface area calculation was done with the program GRASP [A. Nicholls, K. Sharp, B. Honig, *Proteins* **11**, 281 (1991)].
19. A search of the Protein Data Bank with the European Molecular Biology Laboratory DALI server [L. Holm and C. Sander, *J. Mol. Biol.* **233**, 123 (1993)] did not reveal significant structural similarity to any previously determined folds for domains of the flavoprotein other than the flavin binding domain mentioned in the text.
20. C. Hägerhäll and L. Hederstedt, *FEBS Lett.* **389**, 25 (1996).
21. S. K. Shenoy, L. Yu, C. A. Yu, *J. Biol. Chem.* **272**, 17867 (1997); X. D. Yang, L. Yu, D. Y. He, C. A. Yu, *ibid.* **273**, 31916 (1998).
22. J. C. Salerno, H. J. Harmon, H. Blum, J. S. Leigh, T. Ohnishi, *FEBS Lett.* **82**, 179 (1977); T. Miki, L. Yu, C.A. Yu, *Arch. Biochem. Biophys.* **293**, 61 (1992), A. R. Waldeck *et al.*, *J. Biol. Chem.* **272**, 19373 (1997).
23. J. Deisenhofer, O. Epp, K. Miki, R. Huber, H. Michel, *Nature* **318**, 618 (1985); G. Feher, J. P. Allen, M. Y. Okamura, D. C. Rees, *ibid.* **339**, 111 (1989).
24. H. Beinert, B. A. C. Ackrell, A. D. Vinogradov, E. Kearney, T. P. Singer, *Arch. Biochem. Biophys.* **182**, 95 (1977); T. Ohnishi and B. L. Trumpower, *J. Biol. Chem.* **255**, 3278 (1980).
25. T. Ohnishi *et al.*, *J. Biol. Chem.* **256**, 5577 (1981).
26. P. L. Dutton *et al.*, *Biological Electron Transfer Chains: Genetics*, *Composition and Mode of Operation*, G. W. Canters and E. Vijgenboom, Eds. (Kluwer, Netherlands, 1988), pp. 3–7.
27. G. Cecchini, B. A. C. Ackrell, J. O. Deshler, R. P. Gunsalus, *J. Biol. Chem.* **261**, 1808 (1986); B. A. C. Ackrell, B. Cochran, G. Cecchini, *Arch. Biochem. Biophys.* **268**, 26 (1989).
28. P. Mitchell, *Biol. Rev.* **41**, 445 (1966); For a review, see U. Brandt and B. L. Trumpower, *Crit. Rev. Biochem. Mol. Biol.* **29**, 165 (1994).
29. For a review, see M. Saraste, *Science* **283**, 1488 (1999).
30. S. Iwata, C. Ostermeier, B. Ludwig, H. Michel, *Nature*, **376**, 660 (1995); T. Tsukihara *et al.*, *Science* **269**, 1069 (1995).
31. J. P. Abrahams, A. G. W. Leslie, R. Lutter, J. E. Walker, *Nature* **370**, 621 (1994).
32. S. Bailey, *Acta Crystallogr.* **D50**, 760 (1994).
33. J. I. Yeh, A. Claiborne, W. G. Hol, *Biochemistry* **35**, 9951 (1996).
34. K. Fukuyama, N. Ueki, H. Nakamura, T. Tsukihara, H. Matsubara, *J. Biochem (Tokyo)* **117**, 1017 (1995).
35. E. T. Adman, L. T. Sieker, L. H. Jensen, *J. Biol. Chem.* **251**, 3801 (1976).
36. Crystal contacts in the membrane-spanning region of a protein are relatively unusual, but have previously been seen in the structure of the iron transporter FhuA [K. P. Locher, B. Rees, D. Moras, J. P. Rosenbusch, in *G-Protein–Coupled Receptors* T. Haga, Ed. (CRC Monographs, CRC Press, Boca Raton, FL, in press); K. P. Locher *et al.*, *Cell* **95**, 771 (1998)], porins [S. W. Cowen *et al.*, *Nature* **358**, 727 (1992)], and bacteriorhodopsin, which was crystallized in the presence of cubic lipids [E. Pebay-Peyroula, G. Rummel, J. P. Rosenbusch, E. M. Landau, *Science* **277**, 1676 (1997)].
37. All figures were made with MOLSCRIPT [P. J. Kraulis, *J. Appl. Crystallogr.* **24**, 946 (1991)] or BOBSCRIPT [R. Esnouf, *J. Mol. Graph.* **15**, 133 (1997)] and rendered with RASTER3D [E. A. Merritt and M. E. P. Murphy, *Acta Crystallogr.* **D50**, 869 (1994)].

38. Supported by the Department of Veterans Affairs, NIH, and NSF (G.C. and C.L-C.), and the Howard Hughes Medical Institute and NIH (D.C.R.). T.M.I. is supported by an NIH training grant. We thank I. Schröder, S. I. Chan, S. C. Hung, and the members of the Rees group for discussions; K. H. Tubman and T. D. Tubman for critical reading; and J. J. Ottesen and T. N. Earnest for experimental assistance. The Advanced Light Source is supported by the Director, Office of Energy Research, Office of Basic Energy Sciences, Materials Sciences Division, of the U.S. Department of Energy under Contract No. DE-AC03-76SF00098 at Lawrence Berkeley National Laboratory.

3 May 1999; accepted 21 May 1999